# Anomalous carbon clusters in 4H-SiC/SiO$_2$ interfaces

Y. Kagoyama, M. Okamoto (ID), T. Yamasaki, N. Tajima, J. Nara, T. Ohno, H. Yano, S. Harada, and T. Umeda

View Online        Export Citation        CrossMark

# Anomalous carbon clusters in 4H-SiC/SiO₂ interfaces

View Online · Export Citation · CrossMark

Y. Kagoyama,[1] M. Okamoto,[2] T. Yamasaki,[3] N. Tajima,[3] J. Nara,[3] T. Ohno,[3] H. Yano,[1] S. Harada,[2] and T. Umeda[1]

## AFFILIATIONS

[1]Institute of Applied Physics, University of Tsukuba, Tsukuba 305-8573, Japan
[2]Advanced Power Electronics Research Center, National Institute of Advanced Industrial Science and Technology (AIST), Tsukuba 305-8568, Japan
[3]Computational Materials Science Unit, National Institute for Materials Science (NIMS), Tsukuba 305-0044, Japan

## ABSTRACT

We investigated a metal-oxide-semiconductor interface of dry-oxidized $(000\bar{1})$ 4H-SiC, which was known as the most electrically deteriorated SiC MOSFET, by electrically detected magnetic resonance (EDMR) and observed a signal with an isotropic g factor (2.0024) and magnetic-field angular dependent signal widths. Judging from the g factor, the signal comes from $sp^2$-bonded carbon clusters. In addition, we found that the angular dependence of EDMR signal widths was caused by two-dimensional dipolar broadening with exchange interaction between electron spins. However, the density of electron spins or carbon clusters was $5.4 \times 10^{13}$ cm$^{-2}$, which was not high enough for exchange interaction. Therefore, we propose inhomogeneous distribution of carbon clusters in the interface. At the interface, $\pi^\star$ peaks from $sp^2$-bonded carbon atoms were detected by electron energy loss spectroscopy. Scanning the electron beams along the interface revealed uneven existence of the $\pi^\star$ peaks, which also proved that the $sp^2$-bonded carbon atoms were distributed inhomogeneously in the interface. In addition, we found the formation of $sp^2$-bonded carbon clusters at 4H-SiC$(000\bar{1})$/SiO₂ interfaces and interaction between $\pi$-conjugate electron spins on the carbon clusters by first principles calculation. Such carbon clusters generated electrically active states widely in the energy gap of 4H-SiC. The states result in the Fermi level pinning of the MOSFET.

## I. INTRODUCTION

Silicon carbide (4H-SiC) and its metal-oxide-semiconductor (MOS) interfaces have attracted much attention as the heart of next-generation power transistors such as SiC MOS field-effect transistors (MOSFETs).[1] This system also provides a scientifically interesting issue: what types of interface defects are formed using typical covalent-semiconductor elements. The SiC-MOS interfaces are abrupt and simply consist of Si, C, and O atoms.[2] Nevertheless, they exhibit unpredictably wide variations; for instance, the field-effect mobility ($\mu_{FE}$) of the channel of SiC-MOSFETs shows a wide range of degradation from 0 to 100 cm$^2$ V$^{-1}$ s$^{-1}$, depending on surface orientations and oxidation processes.[3–5] The identification of interface defects in this system is a timely issue. Electron spin resonance (ESR) and electrically detected magnetic resonance (EDMR) spectroscopy have so far revealed various interface defects such as carbon clusters (C clusters),[6,7] P$_{bC}$ centers (interfacial carbon dangling bonds),[8,9] Si-vacancy centers,[10] C-face defects,[11] and carbon-related defects.[12]

In this paper, we identify another key defect in the SiC-MOS system, which was found in dry-oxidized 4H-SiC$(000\bar{1})$/SiO₂ interfaces that are known as the most deteriorated SiC-MOS interfaces. In such interfaces, we identified a new EDMR center of $sp^2$-bonded C clusters. This center is essentially different from the C cluster reported previously.[6,7] The previous ESR centers [g factor ($g$) ≈ 2.003] of the C cluster originated from carbon dangling bonds in the clusters, which are characterized by a spatially localized wave function at a single C atom. On the other hand, the present EDMR center of $g$ ≈ 2.003 originates from $\pi$-like electrons in the $sp^2$-bonded C clusters, which are spatially delocalizing over the cluster. As a consequence, our C-cluster signal revealed two-dimensional (2D) dipolar broadening[13,14] as well as 2D exchange interaction between electron spins.[15–17] Normally, the exchange interaction of 2D electron spins was

generally observed when the spin density exceeded $4 \times 10^{14}$ cm$^{-2}$.[15–17] In contrast, the present center exhibited 2D exchange interaction with one order of magnitude lower spin density. This unusual exchange interaction is closely related to the nature of $sp^2$-bonded C clusters. The presence of such C clusters was also evidenced from transmission-electron-microscope (TEM) observation. Furthermore, first-principles molecular dynamics (FPMD) calculations predicted the formation of $sp^2$-bonded C clusters, which is consistent with various experimental results.

## II. METHODS

### A. EDMR sample fabrication

Fully processed $n$-channel lateral C-face 4H-SiC MOSFETs were prepared on a $p$-epitaxial layer of 4°-off 4H-SiC(000$\bar{1}$) surface. Gate oxides were formed by either dry oxidation at 1200 °C (60 nm in thickness) or wet oxidation at 1100 °C (50 nm in thickness). We named the dry-oxidized sample "Dry" and the wet-oxidized one "Wet." The Dry and Wet samples were subjected to a post oxidation anneal with Ar gas at 1100 °C and H$_2$ gas at 1100 °C, respectively. The post oxidation anneal with Ar gas for the dry-oxide MOSFET was for the same thermal history with the wet-oxide MOSFET. The gate length and the width are 5 and 150 $\mu$m, respectively. The source and drain regions were formed by phosphorous ion implantation. The same type of SiC-MOSFETs was studied in our previous papers, and other detailed information on the MOSFETs can be found in Refs. 4 and 11. The two C-face MOSFETs exhibited strikingly different current-voltage characteristics, e.g., $\mu_{FE}$ was quite high (67 cm$^2$ V$^{-1}$ s$^{-1}$) for the Wet sample but was $10^{-8}$ cm$^2$ V$^{-1}$ s$^{-1}$ for the Dry sample.

### B. EDMR setup

We measured EDMR spectra to investigate what type of defects exist at the MOS interfaces of Dry and Wet samples. We adopted the bipolar-amplification-effect (BAE) technique. This technique was developed by Aichinger and Lenahan,[18] enabling us to amplify EDMR signals via a current amplification function of MOSFET itself. The BAE-EDMR setup is shown in Fig. 1. A current source and an EDMR detector are connected to the drain and source, respectively. Using a forward-biased current source ($I_d$), electrons are injected into the MOS interface. We can control the density of electrons that recombine at the interface defects by changing a gate bias ($V_g$), while most of $I_d$ flows into the well region as a well current ($I_w$, see Fig. 1) which is unrelated to the interface defects. We then measured ESR-induced current changes ($\Delta I$) due to the MOS interface defects using the drain-source currents ($I$). For maximizing the signal-to-noise ratio of EDMR signals in the Dry MOSFETs, $I_d$ was set to be 100 $\mu$A, and the $I$ was 750–780 nA, in the $V_g$ range between −30 and +15 V. For the case of the wet MOSFETs, the details of the optimizing EDMR setup were already reported in Ref. 11. All measurements were performed at room temperature and with a microwave of 9.462 GHz and 200 mW. EDMR signals were detected using a
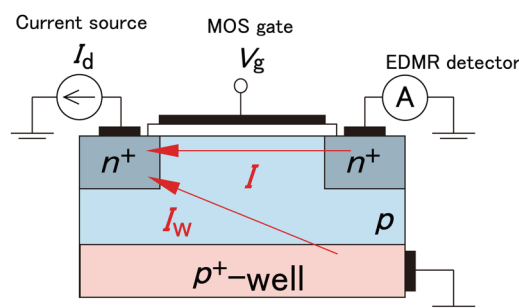


**FIG. 1.** BAE-EDMR setup used for maximizing EDMR signals of MOS interface defects.

lock-in detection synchronized to a magnetic-field modulation at 1.56 kHz. The magnetic-field modulation amplitudes were set to be 0.5 mT for the Dry sample and 0.25 mT or less for the Wet sample.

### C. TEM/EELS setup

Using electron-energy-loss spectroscopy (EELS), we can distinguish $sp^2$- and $sp^3$-bonded C atoms, which are detectable as a π* peak at 285 eV and σ* peak at 290 eV in the C-K energy-loss edge, respectively.[19] The TEM sample (40 nm in thickness) was prepared from the EDMR sample by focused-ion-beam machining. High-resolution TEM/EELS measurements conventionally used an acceleration voltage of over 100 kV (typically 200 kV)[20] and a focused electron beam with a sub-nm diameter. However, such conditions strongly damaged SiC/SiO$_2$ interface regions, as evidenced in a scanning TEM (STEM) image of Fig. 2(a). As is shown in the figure, a 200-kV EELS observation along the interface (indicated by a dashed line) can generate amorphized regions at the interface over the scanning area. Note that such damages were not observed at Si/SiO$_2$ interfaces with similar observation conditions. The amorphized regions showed a strong π* carbon-EELS signal due to the formation of amorphous carbons. Therefore, to minimize such artificial damages, we have optimized the acceleration voltage, beam diameter, scanning steps, and measurement times at each point. STEM images were obtained using a JEOL HEM-ARM 200F electron microscope operated with a low acceleration voltage of 60 kV. The electron beam was defocused into 1 nm in diameter and scanned just along the interface every 2 nm over a 150-nm length. When scanning the beam, the beam position was accurately calibrated relative to the standard position defined inside 4H-SiC lattice image.

We also examined EELS intensity profiles *across* the Dry interface as similarly to the previous work such as Ref. 20. The result is summarized in Fig. 2(b). In this measurement, a higher-resolution condition with a focused electron beam was used: acceleration voltage of 80 kV, beam spot diameter = 0.2 nm, and beam step = 0.2 nm. At every scanning point, we measured intensities of Si-L edge (95−105 eV), C-K edge (285−295 eV), and O-K edge (535−545 eV) in each EELS
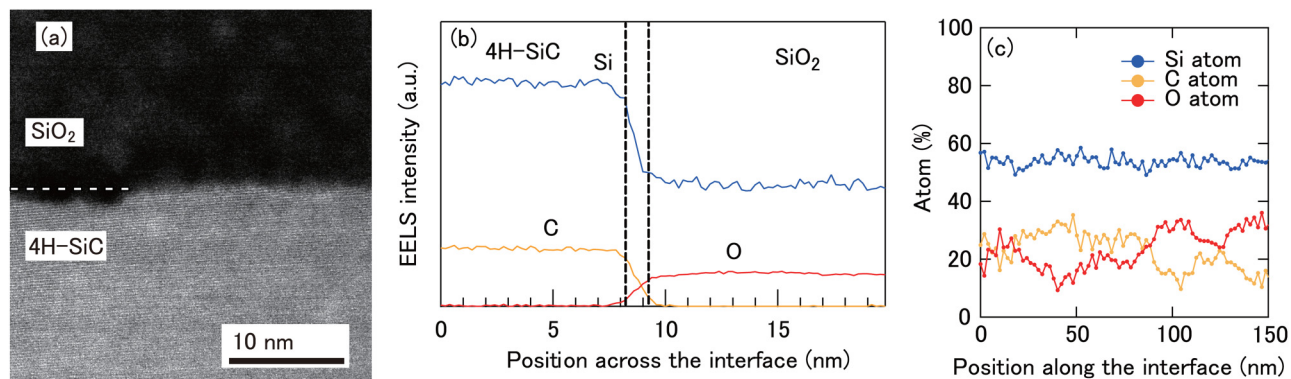
**FIG. 2.** (a) Annular-dark-field STEM image of a 4H-SiC(000$\bar{1}$)/SiO$_2$ interface (the Dry interface) *after* a conventional 200-kV EELS scanning analysis along the interface (indicated by a dashed line). Amorphized damages were induced over the EELS scanning area. (b) EELS intensity profiles *across* the Dry interface measured by a low-damage (80 kV) EELS scanning analysis. (c) Compositional profiles *along* the Dry interface obtained by EDX spectrometry (60 kV). The vertical intensities were normalized by the standardless correction. The horizontal range (0—150 nm) was the same as that shown in Fig. 5(d).

spectrum. The obtained profiles of Si, C, and O indicate an interfacial region of 1-nm width (dashed lines). This interfacial region was much narrower than that shown in the previous work (3—4 nm),[20] suggesting that our TEM/EELS analysis has achieved a lower damage analysis. From this preliminary EELS analysis, we decided that a beam spot was expanded to 1-nm diameter to fully cover the interfacial region and to minimize the damages. If the carbon EELS signal was lost, it should be judged that the beam spot strays off the interfacial region.

In EELS scanning analyses along the interface, we also simultaneously measured energy-dispersive X-ray spectrometry (EDX) to check compositional fractions of Si, C, and O atoms at each scanning point [Fig. 2(c)]. As is seen in the figure, C atoms were always detected, ensuring that the beam spot traced the interface. About 10% fluctuation was present in the compositional fraction of C atoms, although that of Si atoms was almost constant. These profiles may suggest the presence of non-stoichiometric C atoms at the interfacial region. Their density is nominally estimated to be $10^{14}$ cm$^{-2}$ (10% of the interfacial atomic density). However, we must be careful in quantitative arguments, and hence we tried to examine non-stoichiometric C atoms by observing the carbon $\pi^*$ EELS signals, which will be described in Sec. III C.

### D. FPMD simulations

We performed O$_2$ oxidation simulations of 4H-SiC(000$\bar{1}$) using the FPMD program PHASE/0,[21] which is based on the density functional theory[22] with pseudopotentials and plane wave basis. Pseudopotentials for Si and H atoms were norm-conserving, and those for C and O atoms were ultra-soft types. Exchange and correlation effects were taken within the generalized gradient approximation (PBE96). Cut off energies of plane wave basis for wave functions and charge density were 16 and 144 Ry, and the $\Gamma$ point was sampled in the

Brillouin zone. We set the temperature as 2000 K aiming to enhance oxidation reactions at the interface. We executed 14 series of simulations, in each of which a total of 22 O$_2$ molecules were introduced one by one at regular intervals (1 ps for the first 11 O$_2$ and 2 ps for the latter 11 O$_2$) into the interface region. The unit cell of an initial structure model contains a substrate of six SiC bilayers, 6.5-Å thick amorphous-like SiO$_2$ layer smoothly connected to the substrate with no dangling-bond generation, and a 10-Å thick vacuum region, where O atoms at the SiO$_2$ surface and Si atoms at the SiC back surface are terminated with H atoms.

## III. RESULTS AND DISCUSSIONS

### A. EDMR experiments

The EDMR results of Dry and Wet samples are shown in Fig. 3(a). In the Dry sample, a single broad Lorentzian signal appeared at an isotropic g factor of 2.0024. In contrast, the Wet sample revealed sharper anisotropic EDMR signals, which were named "C-face defects,"[11] and they showed a c-axial g tensor of $g_{//}$ = 2.0016 and $g_\perp$ = 2.0023.[11] We tentatively attribute the broadened signal of the Dry sample to high-density 2D electron spins because a similar phenomenon was determined for the P$_b$ centers at Si(111)/SiO$_2$ interfaces, if their density is $\gtrsim 10^{13}$ cm$^{-2}$.[13,14] Such high-density 2D electron spins reveal a broadened ESR signal due to 2D dipolar broadening.[13,14]

Figure 3(b) illustrates a gate-bias ($V_g$) dependence of the EDMR signal in the Dry sample. The EDMR intensity increased linearly with increasing $V_g$ over a very wide range from −30 V to +15 V. This nearly linear response is one of the characteristic features of the EDMR signal in the Dry sample, because EDMR signals of interface defects generally exhibited peak-shaped $V_g$ dependences, as observed in the Wet sample [Fig. 2(c)].[11] Basically, a peak-shaped $V_g$ dependence is associated with a particular energy level of the interface defect; e.g., in Ref. 11, the defect level of the Wet sample was assumed
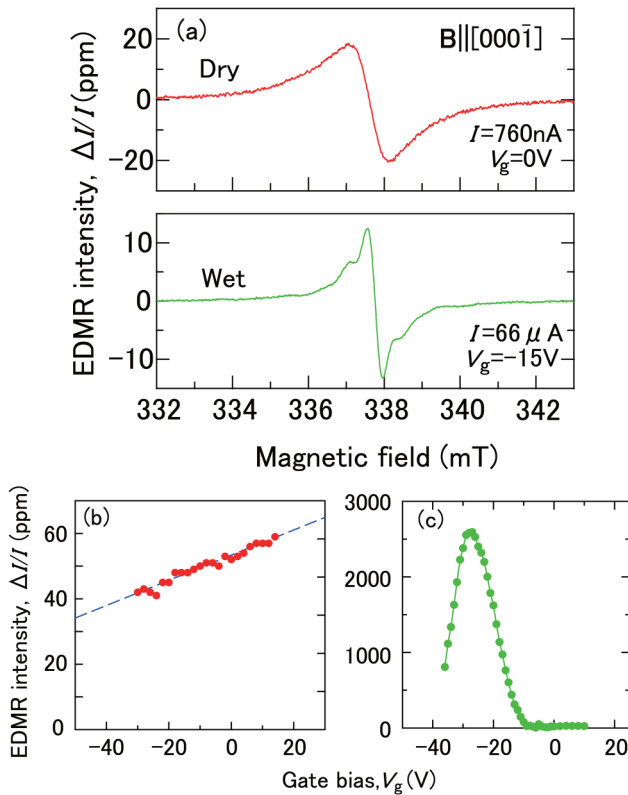
**FIG. 3.** (a) EDMR spectra of "Dry" and "Wet" C-face 4H-SiC MOSFETs for magnetic field (**B**) parallel to [0001]. ESR transitions were excited by a 200-mW microwave at 9.46 GHz. Magnetic-field modulation at 1.56 kHz with an amplitude of 0.25–1.0 mT was used for signal amplification. (b) EDMR signal intensity ($\Delta I/I$) as a function of $V_g$ in the Dry sample, where $\Delta I$ is the peak-to-peak amplitude of current change. (c) $\Delta I/I$ versus $V_g$ in the Wet sample with the defect density of $1.2 \times 10^{13}$ cm$^{-2}$. This graph is the same as Fig. 3(a) in Ref. [11]. The signal intensity was largely enhanced due to a different measurement technique which was optimized for the much high-$\mu_{FE}$ sample.[11]

to be at $E_V$ (valence band edge) + 0.5 eV. Contrary to such a case, we speculate a much broader distribution of the defect levels in the Dry sample. In fact, our theoretical calculations on the C clusters (Sec. III C) predict a broad distribution of their defect levels over the whole range of the energy gap.

At least, by changing $V_g$ from −30 V to +15 V, electrons of $1.6 \times 10^{13}$ cm$^{-2}$ are supplied to the interface, where we calculated $C_{ox}\Delta V/e = 1.6 \times 10^{13}$ cm$^{-2}$ with the oxide capacitance ($C_{ox}$) of $5.6 \times 10^{-8}$ F/cm$^2$, $\Delta V = 45$ V, and $e = 1.602 \times 10^{-19}$ C. These electrons were trapped into the defect levels, forming singly occupied ESR-active states. As a result, the EDMR signal intensity increased. From the observed linear relationship, we roughly estimated a zero EDMR signal at $V_g = -140$ V. This means that the EDMR centers, which act as electron traps and are ESR-active after capturing electrons, may exist by a density of $5.4 \times 10^{13}$ cm$^{-2}$, where $\Delta V$ is 155 V (= 140 + 15 V). This spin density is high enough to cause 2D dipolar broadening. If we

assumed a peak-shaped $V_g$ dependence in a strong negative $V_g$ region ($V_g < -30$ V), the zero EDMR signal could be observed at smaller negative $V_g$ bias, and the defect density could be smaller than the above value. However, we should consider that the defect density in the Dry sample is larger than that in the Wet sample ($1.2 \times 10^{13}$ cm$^{-2}$),[11] judging from the much broader 2D dipolar broadening in the Dry sample.

Figure 4(a) shows the angular dependence of the peak-to-peak width ($\Delta B_{pp}$) of the EDMR signals in the Dry and Wet samples. Both signals revealed angular-dependent signal widths. Such an angular dependence is actually known for 2D dipolar broadening with high-density electron spins ($\gtrsim 10^{13}$ cm$^{-2}$).[13,14] In fact, the dashed lines in the figure were simulated assuming the 2D dipolar broadening [numerically calculating Eq. (5) in Ref. [14]], showing good agreement with the case of the Wet signal. In this simulation, we assumed that the spin density at the Wet interface is $1.2 \times 10^{13}$ cm$^{-2}$, which was experimentally found in Ref. [11]. On the contrary, for the Dry signal, the 2D dipolar broadening cannot account for the experimental result when we assumed the spin density of $\sim 5 \times 10^{13}$ cm$^{-2}$. Even varying the spin density, no good fitting results were obtained.

Instead of simple 2D dipolar broadening, we considered a combination of 2D dipolar broadening and 2D exchange interactions between electron spins. In the case of "ultra-high-density" spins ($> 10^{14}$ cm$^{-2}$), the angular dependence of $\Delta B_{pp}$ is modified by the 2D exchange interactions as follows:

$$\Delta B_{pp} = A + B(3\cos^2\theta - 1)^2,$$

where A and B are constants and $\theta$ is an angle between the magnetic field and the normal of the 2D plane.[15] In fact, the angular dependence of the Dry signal can be well fitted by the above formula, as shown with a solid line in Fig. 4(a) with
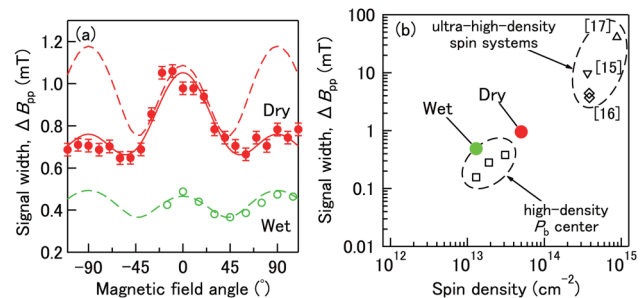


**FIG. 4.** (a) ESR signal width (peak-to-peak widths of first-derivative signals, $\Delta B_{pp}$) as a function of magnetic-field angle $\theta$. Dashed curves were simulated for pure 2D dipolar broadening.[13,14] In addition to 2D dipolar broadening, 2D exchange interaction[15] was taken into account for calculating a solid curve. (b) Relationship between signal widths and 2D spin densities. The left dashed oval indicates the class of pure 2D dipolar broadening observed in high-density $P_b$ centers at Si(111)/SiO$_2$ interfaces.[13] The upper-right dashed oval indicates the class of ultra-high-density spin systems involving 2D exchange interaction, which were observed in 2D magnetic systems.[15–17]

A = 0.99 and B = 0.66 mT. Therefore, we conclude that the Dry signal should involve the 2D exchange interactions, indicating a very short distance between electron spins at the Dry interface.

Interestingly, the present Dry interface is quite unusual compared to the known examples of ultra-high-density 2D spin systems.[15–17] Figure 4(b) shows a relationship between $\Delta B_{pp}$ and 2D spin densities for the high-density $P_b$ systems[14] and the ultra-high-density 2D spin systems.[15–17] The present experimental data are also plotted in the figure. The Wet signal belongs to the class of the high-density 2D spin systems, exhibiting pure 2D dipolar broadening. In contrast, for the Dry signal, its $\Delta B_{pp}$ and spin density approached those of the high-density 2D spin systems; however, the angular dependence of $\Delta B_{pp}$ is similar to that of the ultra-high-density 2D spin systems ($>4 \times 10^{14}\,\mathrm{cm^{-2}}$).

The observed isotropic $g$ factor of 2.0024 in the Dry sample is close to those of the C clusters[6,7] and Si-vacancy center.[10] In addition, similar $g$ factors are commonly observed for other carbon-related interface defects[8,9,11,12] as well as electron spins in various carbon materials.[19] We therefore argue that the present EDMR center is a sort of carbon electron spins. The observed $g$-isotropy suggests a random orientation of electron spins at the Dry interface. For the origin of such carbon electron spins, we propose $sp^2$-bonded C clusters that are inhomogeneously formed at the Dry interface. This model naturally accounts for the random orientation of carbon electron spins. Carbon electron spin(s) may be confined in a C cluster and delocalize over the size of the cluster via a $sp^2$ $\pi$-conjugate electronic system. Such features may promote the 2D exchange interaction even with a low spin density. In addition, an inhomogeneous formation of the C clusters may assist in a spatial condensation of carbon electron spins.

### B. EELS experiments

By optimizing the damage-less TEM/EELS observations described in Sec. II C, we obtained no appreciable structural changes at the interface, which was confirmed by the second TEM observation as shown in Fig. 5(a). In the inset of Fig. 5(a), a lattice image of 4°-off 4H-SiC and an amorphous structure of SiO$_2$ are resolved. At every scanning point [the yellow dots in Fig. 5(a)], we measured C-K edge, O-K edge, and Si-L edge in the EELS spectrum, confirming the presence of all C, O, and Si atoms. It ensures that the electron beam is just located at the SiC/SiO$_2$ interface. We also performed a double check of the co-presence of C, O, and Si atoms in every scanning spot by means of EDX [Fig. 2(c)]. Figure 5(b) shows the C-K edge of the EELS spectra measured at positions A and B in Fig. 5(a). Spectrum A consists of the $\sigma^*$ peak only, while spectrum B includes the $\pi^*$ peak. By scanning 150 points along the interface, scattered $\pi^*$ peaks appeared. This result is reasonably ascribed to the presence of $sp^2$-bonded C clusters at the Dry interface.

The observed C-K edge EELS spectra can be fitted by a combination of $\sigma^*$ and $\pi^*$ peaks. An example is shown at the
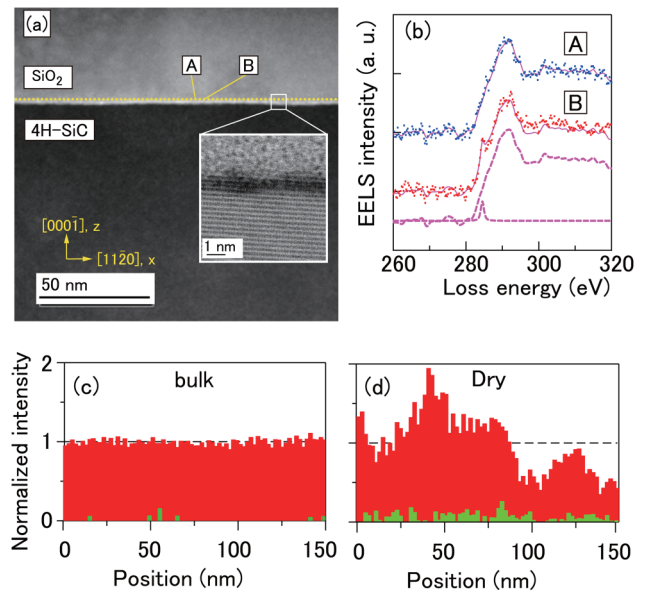


FIG. 5. (a) Cross-sectional annular-bright-field STEM image of the Dry interface. The image shows the ($1\bar{1}00$) plane. Yellow dots along the interface express spots of the 1-nm-diameter electron beam. (b) EELS spectra of C-K edge measured at the spots A and B in (a). (c) and (d) x-direction profiles of $\sigma^*$ (red) and $\pi^*$ (green) intensities measured for a 4H-SiC bulk region and an interface region of the TEM sample, respectively. Intensities were normalized by the average of the $\sigma^*$ peak heights (dashed lines).

bottom of Fig. 5(b). The reference $\sigma^*$ peak was obtained from the average of 76 C-K edge EELS spectra measured for a 4H-SiC bulk region of the same TEM sample. The $\pi^*$ peak was assumed to be always located at 285 eV with a constant width. All C-K edge EELS spectra could be well deconvoluted into these two peaks. We then estimated the distribution profiles of $sp^3$- and $sp^2$-bonded C atoms along the $x$ direction, which are shown with red and green histograms, respectively, in Figs. 5(c) and 5(d). Figure 5(c) was obtained for a 4H-SiC bulk region. Obviously, this region consists of purely $sp^3$-bonded C atoms. On the contrary, in Fig. 5(d), an interface region unambiguously shows the scattered appearance of the $sp^2$-bonded C atoms. This observation supports the inhomogeneous formation of $sp^2$-bonded C clusters at the Dry interface.

Figure 6(a) illustrates such an inhomogeneous formation of the $sp^2$-bonded C clusters. The dots indicate carbon electron spins that are separated by less than 0.3 nm (equivalent to an average spin density of $1 \times 10^{15}\,\mathrm{cm^{-2}}$) to satisfy the observed 2D exchange interactions. The gray areas surrounding the dots express the aggregation of $sp^2$-bonded C atoms, each of which corresponds to C clusters. The density of dots (carbon electron spins) was set to $5 \times 10^{13}\,\mathrm{cm^{-2}}$. As is clear in the figure, the inhomogeneous distribution of the C clusters is indispensable for ensuring 2D exchange interaction. Moreover, we speculate the delocalization of carbon electron spins over the size of each cluster (i.e., each gray areas),
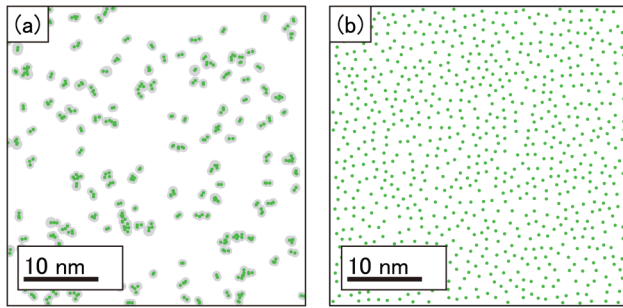
**FIG. 6.** (a) A top view of the $sp^2$-bonded C-cluster model at the Dry interface. The details are given in the text. (b) A top view of the spin distribution in the Wet interface. This distribution was used for calculating the 2D dipolar distribution shown in Fig. 4(a).

further assisting in 2D exchange interaction. On the other hand, in Fig. 6(b), a spin distribution for the Wet interface (the spin density $= 1.2 \times 10^{13} \, \text{cm}^{-2}$) is simulated, which was used for calculating the 2D dipolar broadening shown in Fig. 4(a). Obviously, this type of distribution cannot generate the 2D exchange interactions.

To further check the EELS results, we also performed the same EELS analysis on a 4H-SiC(0001)/SiO$_2$ interface (the so-called "Si-face" interface). The Si-face interface do not show the EDMR/ESR signals of the C clusters.[4,9,10] Furthermore, surface-enhanced Raman spectroscopy strongly suggested that the dry oxidation on the C face generated much stronger graphitic signal (G peak) than on the Si face.[23,24] Therefore, we expected much less appearance of the C $sp^2$ component at the Si-face interface. Figure 7 summarizes our EELS analysis on a dry-oxidized Si-face interface (oxide thickness $= 50 \, \text{nm}$) inside a Si-face 4H-SiC MOSFET. The $\pi^\star$ peak on the Si-face interface was clearly much smaller than the case of Fig. 5(d), supporting our above conclusion and the previous results.[4,9,10,23,24]
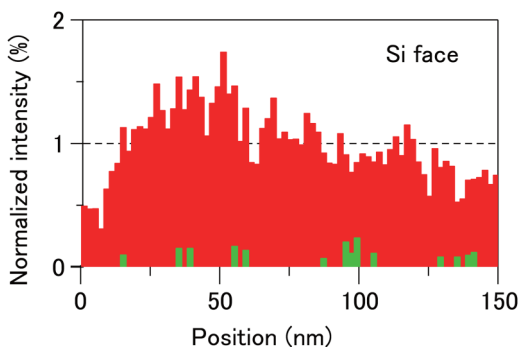
## C. FPMD results

In the FPMD simulation described in Sec. II C, most of the dissociated O atoms from the O$_2$ molecules reacted with the Si atoms and distributed them from the interface to the deeper region of SiO$_2$, and a part of the O atoms generated CO and CO$_2$ molecules with interfacial C atoms. The C atoms left behind at the interface condensed into C clusters. We examined the sizes and configurations of C clusters at the end of the intervals in the period from 15 to 22 O$_2$ molecule introductions. The sizes of C clusters were counted at the ends of intervals in a period of 15 to 22 O$_2$ molecules for the 14 series of the FPMD simulations. The distribution of the sizes of C clusters is shown in Fig. 8(a). Here, we define the size of a C cluster as the number of C atoms contained in the C cluster. The average size of C cluster was 5.4. We also analyzed electronic structures at the ends of intervals and counted gap states that appeared in the SiC energy bandgap. Figure 8(b) shows the correlation between the number of gap states ($n_{\text{gs}}$) and a sum of the number of electrically active C clusters ($n_{\text{C-clusters}}$) and the number of defects ($n_{\text{defects}}$) like $-$Si=O$_2$ and $-$CSi$_3$: the vertical and horizontal axes represent $n_g$ and $n_{\text{c-cluster}} + n_{\text{defects}}$, respectively. Approximately, each active C cluster generates only one gap state.

As an example, Fig. 9(a) shows one of the interface structures obtained after the introduction of 16 O$_2$ molecules among the 14 series. A defect of $-$Si=O$_2$ and four C clusters (two C2 clusters, C5 and C15 clusters) occurred in the interface region. In the energy bandgap of 4H-SiC, three states were generated: $E_V + 0.1 \, \text{eV}$, $E_C - 0.4 \, \text{eV}$, and $E_C$ (to be accurate, this is distributed between $E_C - 0.1$ and $E_C + 0.1 \, \text{eV}$), as shown in Fig. 9(b). The state at $E_V + 0.1 \, \text{eV}$ originated from the $-$Si=O$_2$ defect and was spatially localized, and the state at $E_C - 0.4 \, \text{eV}$ originated from the C15 cluster and was not localized compared to the former one. The state around $E_C$ originated from C15, C5, and C2 clusters and was extended, as indicated by the partial charge density shown in Fig. 9(a). The other C2 cluster [C2$'$ cluster, the second from the left cluster in Fig. 9(c)] gave no bandgap states (we define this kind of C cluster as
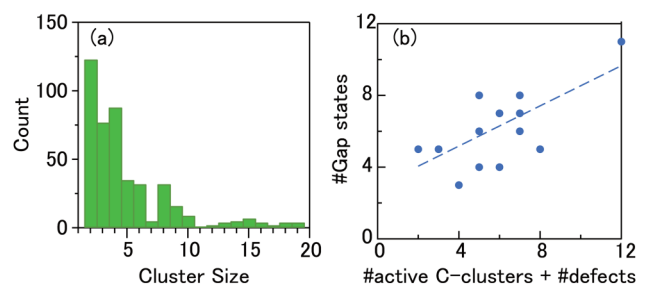


**FIG. 7.** Carbon EELS $\sigma^*$ (red) and $\pi^*$ (green) intensity profiles measured for a dry-oxidized 4H-SiC(0001)/SiO$_2$ interface of a Si-face 4H-SiC MOSFET. We employed the completely same condition and analysis as used for Figs. 5(c) and 5(d).



**FIG. 8.** (a) A distribution of the C cluster size observed at the ends of interval times in a period of 15 to 22 O$_2$ molecules for 14 series simulations. (b) Numbers of gap states appeared in the 4H-SiC bandgap versus summed numbers of active C-clusters and other defects observed for the 14 series of simulations.
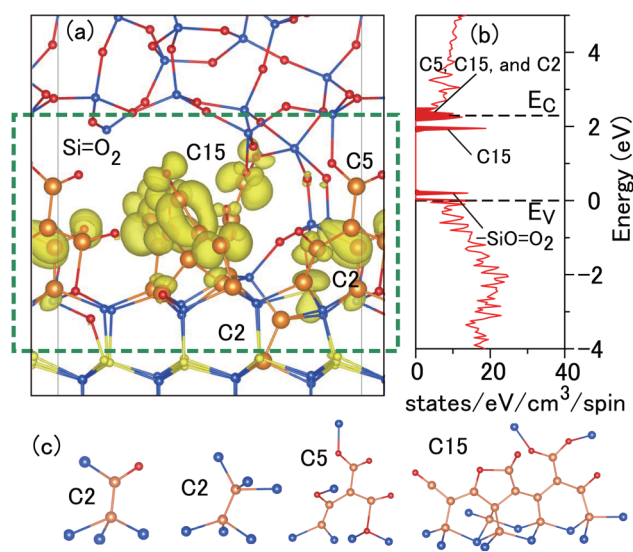
**FIG. 9.** (a) SiO₂/SiC interface structure. Si and O atoms are denoted with blue and red balls, respectively. C atoms in C clusters are orange, and other C atoms are yellow. The superposed yellow isosurface is the charge density integrated from 2.2 eV to 2.4 eV. (b) Calculated density of states in the interface region [the dashed square in (a)]. $E_V$ and $E_C$ are the valence band maximum and the conduction band minimum of 4H-SiC, respectively. (c) Four types of C clusters formed in the interfacial region shown in (a).

"inactive"). All C atoms of the C5 cluster and nine C atoms of the C15 cluster were $sp^2$-bonded. The majority of the C atoms in the C clusters observed among the 14 series were $sp^2$- or $sp$-bonded.

Through the analysis of gap states for the 14 series, we found several interesting features of the $sp^2/sp$-bonded C clusters as follows. (1) Gap states are not carbon dangling-bond states but are delocalized states possibly due to a hybridization of $sp^2$ and $sp$ $\pi$ orbitals. This is consistent with our defect model. (2) The number of gap states correlates to that of electrically active C clusters and defects such as −Si=O₂ and −CSi₃. (3) There is no correlation between the C-cluster size and the number of gap states. Each active C cluster generates approximately only one gap state. Therefore, the theoretical calculation suggests that 2D exchange interactions may be mainly caused between close C clusters, such as among C2, C5, and C15 shown in Fig. 9(a). (4) Electrically active C clusters generate gap states over a wide range of the 4H-SiC bandgap, independent of the C-cluster size and their structures. These gap states can capture electrons, resulting in a Fermi-level-pinning phenomenon, as observed in the Dry interface.

## D. Comparison between the Dry and the Wet samples

The reason why the C clusters are so much formed at the Dry interface is supposedly related to the fast oxidation rate of the C face.[25] Faster oxidation generates more excess C atoms at the interface,[25] enhancing the formation of C clusters.

The large-scale classical MD simulation (which uses the interatomic potentials developed with our FPMD simulation) predicted the formation of various-sized and various configurations of C clusters at a 4H-SiC(000$\bar{1}$)/SiO₂ interface much more dominantly than at a 4H-SiC(0001)/SiO₂ interface.[26] In contrast with dry oxidation, wet oxidation seems to prevent the formation of C clusters, alternatively forming point-defect-like interface defects, as shown in Fig. 6(b). Although our FPMD simulation did not sufficiently examine wet oxidation (introducing H₂O instead of O₂), a preliminary result suggests that the formation of C−H bonds may disturb the aggregation of C atoms. Clarifying atomistic mechanisms in wet oxidation will be the next challenge.

## IV. SUMMARY

In summary, we observed $sp^2$-bonded C clusters at a dry-oxidized 4H-SiC(000$\bar{1}$)/SiO₂ interface by using EDMR and TEM/EELS. They were dominant interface defects at the worst-quality SiC-MOS interfaces. We found the characteristic nature of the $sp^2$-bonded C clusters, e.g., 2D exchange interaction even with a low spin density. The formation of the $sp^2$-bonded C clusters and their characteristic features were revealed from FPMD simulation, which supports the experimental findings.

## REFERENCES

[1]S. Harada, M. Kato, K. Suzuki, M. Okamoto, T. Yatsuo, K. Fukuda, and K. Arai, IEDM Tech. Dig., 903 (2006).
[2]H. Watanabe, T. Hosoi, T. Kirino, Y. Kagei, Y. Uenishi, A. Chanthaphan, A. Yoshigoe, Y. Teraoka, and T. Shimura, Appl. Phys. Lett. **99**, 021907 (2011).
[3]G. Y. Chung, C. C. Tin, J. R. Williams, K. McDonald, R. K. Chanana, R. A. Weller, S. T. Pantelides, L. C. Feldman, O. W. Holland, M. K. Das, and J. W. Palmour, IEEE Electron Device Lett. **22**, 176 (2001).
[4]T. Umeda, M. Okamoto, R. Kosugi, R. Arai, Y. Sato, S. Harada, T. Makino, and T. Ohshima, ECS Trans. **58**, 55 (2013).
[5]T. Kimoto and J. A. Copper, *Fundamentals of Silicon Carbide Technology: Growth, Characterization, Devices, and Applications* (Wiley, Singapore, 2014), Chap. 6.
[6]V. V. Afanas'ev, F. Ciobanu, S. Dimitrijev, G. Pensl, and A. Stesmans, Mater. Sci. Forum **483–485**, 563 (2005), and references therein.
[7]P. J. MacFarlane and M. E. Zvanut, J. Appl. Phys. **88**, 4122 (2000).

[8]J. L. Cantin, H. J. von Bardeleben, Y. Shishkin, Y. Ke, R. P. Devaty, and W. J. Choyke, Phys. Rev. Lett. **92**, 015502 (2004).

[9]T. Umeda, G.-W. Kim, T. Okuda, M. Sometani, T. Kimoto, and S. Harada, Appl. Phys. Lett. **113**, 061605 (2018).

[10]C. J. Cochrane, P. M. Lenahan, and A. J. Lelis, J. Appl. Phys. **109**, 014506 (2011).

[11]T. Umeda, M. Okamoto, H. Yoshioka, G.-W. Kim, S. Ma, R. Arai, T. Makino, T. Ohshima, and S. Harada, ECS Trans. **80**, 147 (2017).

[12]G. Gruber, J. Cottom, R. Meszaros, M. Koch, G. Pobegen, T. Aichinger, D. Peters, and P. Hadley, J. Appl. Phys. **123**, 161514 (2018).

[13]A. Stesmans and B. Nouwen, Phys. Rev. B **61**, 16068 (2000).

[14]K. L. Brower and T. J. Headley, Phys. Rev. B **34**, 3610 (1986).

[15]P. M. Richards and M. B. Salamon, Phys. Rev. B **9**, 32 (1974).

[16]H. R. Boesch, U. Schmocker, F. Waldner, K. Emerson, and J. E. Drumheller, Phys. Lett. **36A**, 461 (1971).

[17]S. Kuroda, K. Marumoto, H. Kihara, H. Ofuchi, M. Tabuchi, Y. Takeda, A. G. Banshchikov, N. S. Sokolov, and N. L. Yakovlev, Jpn. J. Appl. Phys. **40**, L1151 (2001).

[18]T. Aichinger and P. M. Lenahan, Appl. Phys. Lett. **101**, 083504 (2012).

[19]J. Robertson, Mater. Sci. Eng. R **37**, 129–281 (2002).

[20]K.-C. Chang, Y. Cao, L. M. Porter, J. Bentley, S. Dhar, L. C. Feldman, and J. R. Williams, J. Appl. Phys. **97**, 104920 (2005).

[21]T. Ohno, T. Yamamoto, T. Kokubo, A. Azami, Y. Sakaguchi, T. Uda, T. Yamasaki, D. Fukuta, and J. Koga, in Proceedings of the 2007 ACM/IEEE Conference on Supercomputing (SC'07) (2007), No. 57, see https://azuma.nims.go.jp/

[22]W. Kohn and L. J. Sham, Phys. Rev. **140**, A1133 (1995).

[23]S. H. Choi, D. Wang, J. R. Williams, M. Park, W. Lu, S. Dhar, and L. C. Feldman, Appl. Surf. Sci. **253**, 5411 (2007).

[24]W. Lu, L. C. Feldman, Y. Song, and S. Dhar, Appl. Phys. Lett. **85**, 3495 (2004).

[25]D. Goto and Y. Hijikata, J. Phys. D **49**, 225103 (2016).

[26]S. Takamoto, T. Yamasaki, T. Ohno, A. Hatano, and S. Izumi, J. Appl. Phys. **123**, 185303 (2018).